International Journal of Computer Information Systems and Industrial Management Applications
ISSN 2150-7988 Volume 18(23s) 2026 pp. 672-685
https://doi.org/10.70917/ijcisim-2026-5631
Article

Optimized Faster Region Convolutional Neural Hybrid Kernel Multi-Birth Support Vector Machine for Pulmonary Disease Detection

S.Deepankumar[1], Dr. R.MaruthaVeni[2]

[1]Research Scholar, Department of Computer Science, Dr. SNS RajaLakshmi College of Arts and Science, Coimbatore, Tamil Nadu, India. deepankumarmca3@gmail.com
[2]Associate Professor, Department of Computer Science, Dr. SNS RajaLakshmi College of Arts and Science, Coimbatore, Tamil Nadu, India. mveni.r.cs@drsnsrcas.ac.in

Abstract: Accurate and early detection of pulmonary diseases is critical for controlling their spread and improving treatment outcomes. The standard molecular, antigen, and antibody tests are ineffective for early detection due to their longer testing duration and being expensive. Chest X-ray and Computed Tomography (CT)-based imaging methods can complement the standard techniques for early detection, but bias may easily affect them, resulting in lower sensitivity. Employing suitable Deep Learning (DL) methods with effective bias control can accurately identify the pulmonary disease patterns in the images within less time. This paper proposes an Optimized Faster Region-Convolutional Neural Hybrid Kernel Multi-Birth Support Vector Machine (OFRCN-HKMBSVM) classifier for improved pulmonary disease detection. With the minority class imbalance problem resolved by modifying the loss function with class weight adjustment, this model combines the Faster Region Convolutional Neural Networks (F-RCNN) and advanced Machine Learning (ML) model of Hybrid Kernel Multi-Birth Support Vector Machine (HKMBSVM) to detect the severity of pulmonary diseases without bias. This model extracts the region-based features from the pre-processed images using the F-RCNN utilizing the ResNet50 as the backbone model, whose last layer is replaced with HKMBSVM. This combination maps complex pulmonary disease patterns such as opacities, consolidations, or ground-glass patterns and identifies the linear and non-linear relationships between them to differentiate different pulmonary diseases. A hybrid kernel combining polynomial and Bessel kernel functions and the Red-billed Blue Magpie Optimizer (RBMO)--based hyperparameter tuning of the model helps achieve the objective. Evaluation results showed that the OFRCN-HKMBSVM-based model improved the early detection of pulmonary diseases with reduced bias and inference time.
Keywords: Pulmonary Diseases, COVID-19, Deep Learning, Faster Region Convolutional Neural Networks, Multi-Birth Support Vector Machine, Bessel Kernel, Red-billed Blue Magpie Optimizer

1. Introduction

The detection of pulmonary diseases is important to decrease the mortality rate and increase the treatment for the diseases. Early diagnosis helps prompt medical intervention for conditions including lung tumor, tuberculosis, COVID-19, and pneumonia [1]. Conventional methods such as molecular tests, antibody detection, and antigen-based assays are utilized for disease detection. The molecular tests identify the genetic material of pathogens by utilizing amplification techniques such as Reverse Transcription Polymerase Chain Reaction (RT-PCR) to diagnose bacterial and viral infections. The antibody test identifies the body's immune response to an infection by detecting the antibodies, namely IgM and IgG, in blood samples. The Antigen-based assays identify particular antigens (proteins) from a pathogen and are used for quick diagnostic tests performed on nasal, throat, and sputum samples. These tests are effective for screening infections in larger samples and differentiate between various strains of the virus. However, these tests are expensive with longer processing time, and have limitations to detect early stage of the disease.

The ML and DL models used in medical image analysis increase the efficiency and precision of pulmonary disease detection. These models identify the patterns and mappings in the medical images and help in disease identification and severity assessment [2]. However, these diagnostic methods have limitations, including class imbalance, inability to collect relevant disease patterns, computational complexity, higher requirement of resources, and higher inference time. To overcome these limitations, the optimized hybrid model is required, which increases the robustness and effectiveness of pulmonary disease detection. This paper develops a hybrid model Optimized Faster Region-Convolutional Neural Hybrid Kernel Multi-Birth Support Vector Machine (OFRCN-HKMBSVM) classifier which integrated Faster Region-Convolutional Neural Networks (F-RCNN) with the Hybrid Kernel and Multi-Birth SVM for pulmonary disease detection. The F-RCNN model is used as the feature extractor, identifying regions of interest (ROI) within an image and focusing on regions that show disease-related abnormalities. This process also captures detailed spatial and contextual features from the identified regions using ResNet50 architecture. The HKMBSVM is the classification method for differentiating between different pulmonary diseases. The hybrid kernel combines polynomial and Bessel kernel, providing flexibility in mapping different imaging data. The Multi-birth SVM utilizes multiple hyperplanes for classification, ensuring better separation of complex lung diseases. The F-RCNN and SVM components, such as weight and bias, are optimized using the Red-Billed Blue Magpie Optimizer (RBMO) algorithm. This model increases the detection and provides scalable and effective diagnostics in diverse clinical settings. The key contributions of this paper include

- The hybrid model combined F-RCNN with HKMBSVM, which enabled better feature mapping for classifying pulmonary diseases and increased diagnostic accuracy.
- The hybrid kernel combined Bessel and polynomial kernels increases the model capability to characterize between fine changes in medical images.
- The model parameters are tuned using RBMO, which reduces computational complexity, inference time, and resource requirement and increases detection accuracy.

The remainder of the paper is organized as: Section 2 describes related methodologies for pulmonary disease detection and the results are discussed in section 4 while the conclusions are given in section 5.

2. Related Works

Bhandari et al. [3] presented a lightweight CNN model combined with XAI architecture. The model resized the images, flipped the images horizontally, and normalized the pixels. The CNN model is used to collect feature patterns, and the XAI framework uses three algorithms. Algorithms such as Shapley additive explanation (SHAP) measure the feature influence, Local Interpretable Model-agnostic Explanation (LIME) identifies the absence and presence of continuous patches, and Gradient-weighted Class Activation Mapping (Grad-CAM) produces the heatmap to highlight areas. The model collected data from public datasets and classified it into normal, COVID19, Tuberculosis, and Pneumonia. The model attained 95.94% average accuracy, and for pneumonia, 97.26% precision, 96.53% F1 score, and 96.19% recall. However, the CNN-XAI has increased complexity due to XAI algorithms. Ravi et al. [4] developed a Multichannel EfficientNet-Based Stacking Ensemble Learning (MCESEL) Model. The collected data is normalized and resized. The features are collected using the multichannel model that includes Efficient-B0, B1, and B2. The SEL model used logistic regression as a Meta classifier, random forest as a base classifier, and binary cross-entropy loss for training. The model collected data from public datasets and attained 98% recall, F1 score, accuracy and precision for COVID-19, 0.99 accuracy, 0.98 F1 score, precision, and recall for pneumonia, and 99% F1 score, recall, accuracy, and precision for TB. Yet, the model does not gather the important features. Goyal et al. [5] developed a Feature-Enhanced Recurrent Neural Network with Long Short-Term Memory (F-RNN-LSTM) model. The F-RNN-LSTM used median filtering for noise elimination and intensity adjustment for standardization. The Histogram of Oriented Gradients (HOG) captured the patterns, and ROI intensity normalized the features. The RNN with LSTM model is employed for classification. The model evaluated on the C19RD dataset and attained 95.04% accuracy, 95.19% F1 score, 96.78% recall, 93.65% precision, and1289s training time. Yet, the model fails to retain the features during

feature normalization. Rajagopal et al. [6] presented a Deep Convolutional Spiking Neural Network optimized with Arithmetic Optimization Algorithm (DCSNN-AOA). The noises are eliminated and the image is enhanced using the Anisotropic Diffusion Filter-Based Unsharp Masking and Crispening (ADF-UMC). The features are collected by applying Empirical Wavelet Transform (EWT). The model is classified using DCSNN and tuned using AOA. The model used the NIH CXR dataset and attained 96.25% accuracy, 93.61% precision, 97.74% recall, 91.09% F1 score, and 98.52% specificity. Yet, the model has increased complexity. Mezina et al. [7] proposed a Vision Transformer-based neural network that combines InceptionV3 and Transformer architecture. The model segmented the image using a U-Net model and augmented the data. The features are collected using InceptionV3 and Vision Transformer to collect the finer details. The MLP classified the images using the collected features. The model used the ChestX-ray14 dataset and attained 0.8119 AUC, 73.21% accuracy, 76.83% Recall, 72.21% specificity, 32.19% precision, and 42.60% F1 Score.

Bhosale et al. [8] presented DWTMBConvNet architecture by integrating Discrete Wavelet Transform (DWT) with Mobile Inverted Residual Bottleneck Convolution (MBConv) blocks. The DWT collected the frequency and location features from the images. The MBConv blocks incorporate Pointwise convolution, Depthwise convolution, and Squeeze-and-Excitation (SE) blocks for channel-wise feature recalibration. The model sourced the images from a public database and obtained 95.5% accuracy, 95.5% sensitivity, 98.9% specificity, and 95.5% F1 score. Yet, the model lacks in pre-processing steps. Harale et al. [9] developed an improved YOLOv5 for detection and CNN with SVM for classification. The model collected the data and scaled the image for consistent. The YOLOv5 model architecture is enhanced using Spatial Pyramid Pooling with Feature Concatenation (SPPF), Concatenation, and upsampling layer for detection. For classification, the CNN-SVM architecture utilizes the features collected using the CNN layers and classified by applying the SVM classifier with a regularization coefficient. The model used LIDC-IDRI and attained 95.49% precision, 94% recall, 86.40% mAP for iYOLOv5 and 89.51% precision, 86.6% recall, 0.9805 F1 score, and 0.9817 accuracy. Yet, the model is dimensionally constrained. Lin et al. [10] developed an enhanced ant colony optimization algorithm (ACO) and fuzzy k-nearest neighbors (FKNN) and transfer functions for binary feature selection called bIPCACO-FKNN. The ACO is improved by applying an incremental proportional-integral-derivative (PID) control technique for convergence capabilities. The wrapper-based feature selection method selected the relevant features. The transfer functions with the bIPCACO-FKNN model optimized detection. The data is sourced from the Affiliated Hospital of Wenzhou Medical University and attained 98.196% accuracy, 99.50% specificity, 99.67% precision, and 98.56% F1 score. Yet, the model does not optimally balance selected features precision and quantity.

3. Methodology

The research collected chest X-ray (CXR) and CT images and preprocessed the images to increase contrast. Pixel intensities are scaled to a consistent range, which increases the model's capability to generalize. The pre-processed images are used for region proposal and the features are collected in the FRCNN model. The RPN identifies the region that contains abnormalities and generates bounding boxes around these regions. The features are captured from the regions using the convolutional layers (CL) that focus on the Pulmonary Disease mapping and patterns. The deep CL captures the ROI's hierarchical features, including spatial and textural patterns. The captured features are passed to the HKMBSVM classifier, which uses a hybrid kernel to map the characteristics into the high-dimensional spaces. The hybrid kernel distinguishes pulmonary diseases like COVID-19, tuberculosis, lung cancer, and pneumonia with high precision. The model employed the Multi-Birth SVM instead of a single decision boundary to improve the class separation. This technique handles the overlapping patterns between respiratory conditions, and the loss function is adjusted to assign higher penalties using a class weight adjustment technique that reduces misclassifications. Fig 1 represents the overall flow diagram of the OFRCN-HKMBSVM model.

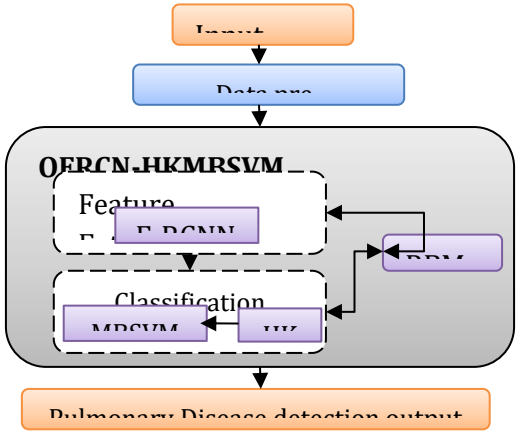

Fig 1. Overall flow diagram of OFRCN-HKMBSVM model

3.1 Dataset Description

The OFRCN-HKMBSVM model employed the Iraq-Oncology Teaching Hospital-National Centre for Cancer Diseases called IQ-OTH-NCCD lung cancer dataset and lung diseases datasets from Kaggle combining COVID-19, tuberculosis, lung cancer, bacterial pneumonia, viral pneumonia and normal samples. The collected dataset contains a total of 18000 images. Each disease class contains 3000 images along with 3000 normal samples. All images are pre-processed and labeled using experts.

3.2 Pre-processing methods

The Chest X-rays and CT scan images are collected that include different lung diseases, which ensures balanced representation. The collected images are converted into a uniform format to ensure consistency, and the images are resized to fixed resolutions that reduce the computational complexity. The pixel intensity values in the images are scaled to a specific range that demonstrates uniformity.

3.3 Proposed Method

The processed images are given to the Faster R-CNN (F-RCNN) model. The F-RCNN framework identifies and isolates regions likely to contain abnormalities related to lung disease. Fig 2 illustrates the architecture of the FRCN-HKMBSVM model. The system begins with pre-processing a CXR image that serves as the foundation for regions for detecting lung abnormalities. The ResNet50 extracts the feature maps from the input image that encodes spatial and contextual information. The processed CXR image is fed as input to provide a feature map with high abstractions. This process structure mitigates the vanishing gradient and captures the deeper representations from the image. The ResNet50 uses residual connections that are defined as

$$H(x) = F(x) + x \tag{1}$$

Here, $F(x)$ refers to the transformation applied to the input (x) using the convolutional layers, $H(x)$ refers to the output of the block. This process ensures that the network learns residual mappings $\big(F(x)\big)$ for efficient gradient flow. The ResNet50 processes the processed image through multiple convolutional layers that provide the feature map with $H \times W \times C$ dimensions. Here, H, W refers to the height and weight in spatial dimensions, and C indicates the channels.

The F-RCNN model combines a region proposal network (RPN) with a feature extractor and layer to detect a region of interest (ROI). The RPN process includes sliding windows, bounding box regression, and non-maximum suppression (NMS). The sliding window is employed to the feature map, and at each window position, aspect ratios and multiple anchor boxes of different scales are defined. The anchors are pre-defined bounding boxes of diverse scales placed at the position of the feature map. Each anchor is parameterized as

$$A = (x_a, y_a, w_a, h_a) \tag{2}$$

Here, (x_a, y_a) refers to the center coordinates and (w_a, h_a) refers to the width and height. For each anchor box, the RPN detects the object score (P_{obj}), which indicates the probability that the anchor contains an object. The object score is estimated using a binary classifier that is defined as

$$P_{obj} = \sigma(W_{obj}F + b_{obj}) \tag{3}$$

Here, W_{obj} refers to the weight matrix and b_{obj} refers to the bias term. The bounding box adjustments are used to refine anchor box dimensions. In the bounding box refinement, the anchor boxes are adjusted using predicted offsets given as

$$\tilde{a} = a + \Delta x.w \tag{4}$$

$$\tilde{b} = b + \Delta y.h \tag{5}$$

$$\tilde{p} = p.e^{\Delta w} \tag{6}$$

$$h' = h.e^{\Delta h} \tag{7}$$

Here, (a, b, p, h) indicates the anchor box center and dimensions, $\tilde{a}, \tilde{b}, \tilde{p}, h'$ indicates the refined coordinates, and $\Delta x, \Delta y, \Delta w, \Delta h$ refers to the bounding box regression offsets.

NMS technique removes redundant boxes with high overlap using Intersection-over Union (IoU) thresholds given by

$$IoU = \frac{overlap_{area}}{union_{area}} \tag{8}$$

The RPN optimizes a multi-task loss that includes classification loss (L_{cls}) and Localization loss(L_{reg}). The classification loss evaluates the accuracy of objectiveness prediction, expressed as

$$L_{cls} = -\frac{1}{N_{cls}}\sum_i \quad [y_i' \; log \; log \; (O_i) + (1 - y_i') \; log \; log \; (1 - O_i) \;] \tag{9}$$

Here, O_i refers to the predicted objectness score and y_i' refers to the ground truth label.

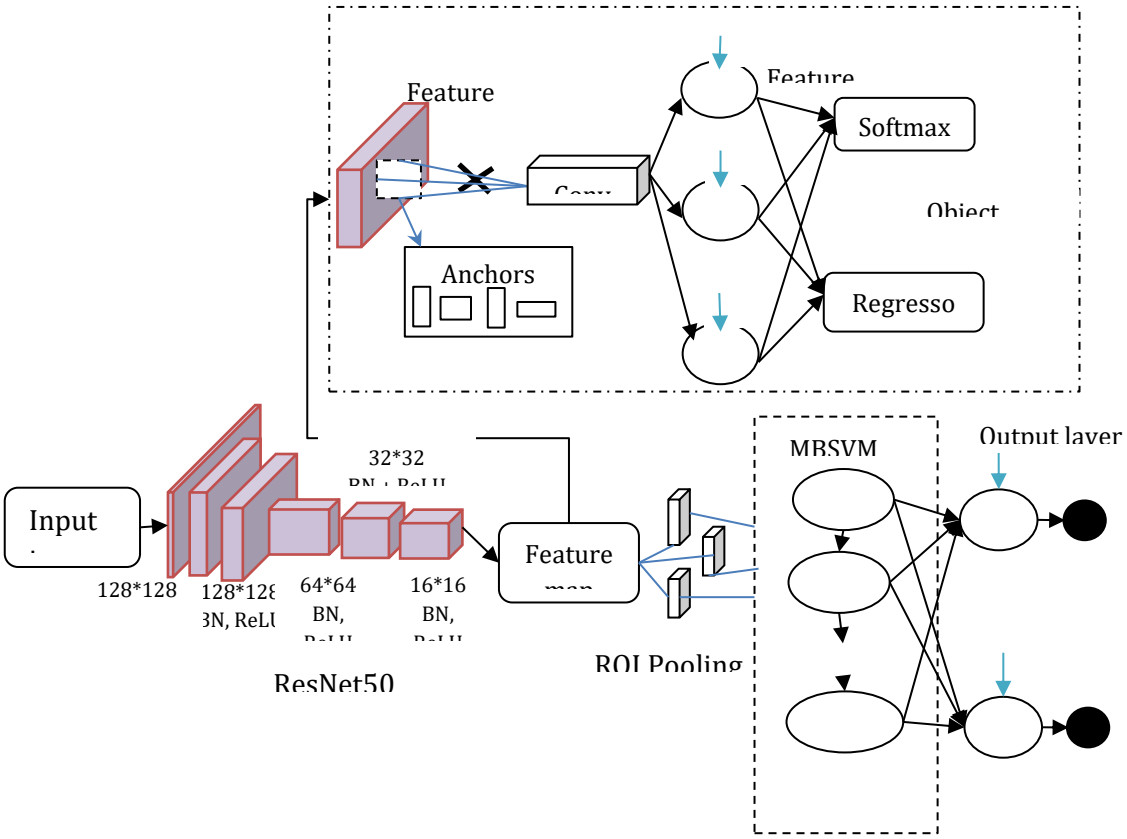

Fig 2. Architecture of OFRCN-HKMBSVM model

The localization loss measures the accuracy of bounding box adjustments, and it is given as

$$L_{reg} = \frac{1}{N_{reg}} \sum_i \quad L1(bp_i - bp_i^*) \tag{10}$$

The combined loss is formulated as

$$L_{RPN} = L_{cls} + L_{reg} \tag{11}$$

The ROI pooling by the RPN is pooled into fixed sizes for processing, and the ROI pooling is that all ROIs have consistent dimensions. The last layer of the ResNet50 is replaced with Multi-birth SVM for classification. The multi-birth SVM leverages classification accuracy using a hybrid kernel that captures the linear and non-linear relationships from the extracted features [11]. The multi-birth SVM replaces the final fully connected layers of ResNet50 and employs multiple hyperplanes for better separation of complex data distributions. The Multi-birth SVM is used to reduce the marginal and classification errors. The hyperplane separates the positive and negative classes of lung diseases. For MB class in Multi-birth SVM, a hyperplane close to the class patterns and one class that is far from all class patterns. The farthest point (class) from the hyperplane is used for decision-making in Multi-birth SVM to classify the various forms and severity of lung diseases. In Multi-Birth SVM, the multi-class point is the severity level derived from the retrieved characteristics. The features from the F-RCNN are presented in the matrix form. For

example, MB denotes the number of classes N_M denotes the number of data points in the MB^{th} class and $x_{MB} \in R^{N_M \times n}, MB = 1,2, \dots, MB$ denotes the patterns of a matrix that belongs to the MB^{th} class. The patterns of the matrix are defined as

$$U_{MB} = \left[x_1^T, \dots, x_{M-1}^T, x_{M+1}^T, \dots, x_M^T\right]^T \quad (12)$$

Here, $U_{MB} \in R^{(N-N_M)\times n}$ denotes the pattern matrix except the MB^{th} class from all the classes, and T denotes the transpose function. The Multi-Birth SVM explores for MB hyperplane for each class and the MB^{th} hyperplane is expressed as

$$MB: (w_{MB}.x) + b_{MB} = 0 \quad (13)$$

Here, w_{MB}denotes the hyperplane weight vector, b_{MB} denotes to the bias, and x denotes to the input vector. For each class(MB), the objective function Multi-birth SVM is expressed as

$$MBSVM = \frac{1}{2} \|U_{MB}w_{MB} + e_{MB1}b_{MB}\|^2 + C_{MB}e_{MB2}^T \varepsilon_{MB} \quad (14)$$

Subject to$x_{MB}w_{MB} + e_{MB2}b_{MB} + \varepsilon_{MB} \geq e_{MB2}, \varepsilon_{MB} \geq 0$ (15)

Here, e_{MB1} and e_{MB2} denotes the vectors of ones, ε_{MB} denotes the slack variable.

The multi-birth SVM is applied to reduce the error sum variables to minimize the pattern misclassification by including MB^{th} $class$ and to reduce the squared distance sum from the hyperplane to the patterns by excluding the MB^{th} class. From the hyperplane, MB^{th} class patterns are set at a distance with the soft margin loss, and this process is set as a rule for the objective function in the multi-birth SVM. The decision function is used to classify the new patterns. The distance to each of MB hyperplanes is computed for the new input $\tilde{x}$. The absolute value $|(w_{MB}.\tilde{x}) + b_{MB}|$ is applied to determine the distance and $\|w_{MB}\|$is applied to normalize the distance. This function is given to the distant hyperplane, and the decision function is formulated as

$$f(x) = \frac{|(w_{MB}.\tilde{x})+b_{MB}|}{\|w_{MB}\|} \quad (16)$$

Here, $|.|$ denotes the absolute value. The Lagrangian function enables multi-birth to solve intricate multi-class classification issues. It encompasses all the multi-birth SVM algorithm's rules and objectives and transforms the initial optimization issue addressed using optimization techniques.

The hybridized kernel improves the multi-birth capacity to recognize intricate and non-linear relationship patterns in the data. The polynomial kernel prioritizes the data partition and uses the Bessel kernels as smooth and oscillatory functions. These kernels are formulated for input $(x_i.\tilde{x}_i)$ as follows:

Polynomial kernel: $K(x_i.x'_i) = (\eta \times (x_i.x'_i) + \delta)^d$ (17)

Bessel Kernel: $k(x_i.x'_i) = \frac{2^v \urcorner(v+1)}{\|x-z\|^v} J_v(\|x-z\|)$ (18)

Here, η, δ and d denotes the kernel parameters, J_v denotes the Bessel function in the order $\left(\frac{(k-1)}{2} \geq 0, k = 1,2 \dots\right)$, $\|.\|$ denotes the Euclidean vector norm, and $\urcorner(.)$ denotes the gamma function. The kernel parameters define the filter size to be applied in the classifier. The classifier's performance is further improved by combining the advantages of kernel functions into a hybrid kernel function. The hybrid kernel called the polynomial-Bessel kernel is formulated as

$$K_{pb} = \beta_1.(\eta \times (x_i.x'_i) + \delta)^d + \beta_2.\frac{2^v \urcorner(v+1)}{\|x-z\|^v} J_v(\|x-z\|) \quad (19)$$

Here, $\beta = [\beta_1, \beta_2]$ is a vector with $\beta_1 + \beta_2 = 1$ and $\eta, \delta, d > 0$. To improve the minority class samples in the class imbalance problem, the loss function is adjusted by allocating higher weights to minority class errors. The weighted loss function for multi-class problems is formulated as

$$L_{weighted} = -\frac{1}{N}\sum_{i=1}^{N} \quad wy_i.log\ log\ (py_i) \tag{20}$$

Here, N indicates the total number of samples, y_i denotes the true class label, py_i denotes the predicted probability for the true class and wy_i denotes the class weight.

The SiLU function reduces the overfitting and introduces smooth gradient flow. This function is formulated as

$$SiLU(x) = x.\sigma(x) \tag{21}$$

Here, x denotes the input to the activation function, and $\sigma(x)$denotes the sigmoid function. The loss function includes class weights and SiLU activation function

$$L = -\frac{1}{N}\sum_{i=1}^{N} \quad wy_i.log\ log\ \left(\sigma\big(SiLU(zy_i)\big)\right) \tag{22}$$

Here, zy_i refers to the pre-activation output for the true label and $\sigma(.)$ denotes the sigmoid activation applied to the SiLU output. The final objective function of FRCN-HKMBSVM is formulated as,

$$f(x) = \frac{1}{2}\ \|\emptyset(X)w_{MB} + e_{MB1}b_{MB}\|^2 + C_{MB}e_{MB2}^T\ \varepsilon_{MB} + K_{pb} + L \tag{23}$$

This HKMBSVM classifier improves the flexibility and ability of the model to handle complex patterns in lung disease detection to increase accuracy and generalization.

The F-RCNN and HKMBSVM hyperparameters are optimized using the RBMO algorithm. The hyperparameters include objective parameters such as margin parameter, kernel parameter in HKMBSVM, and weight, bias, number of layers, and learning rate in F-RCNN. The RBMO algorithm imitates red-billed blue magpies' hunting, cooperative, and food storage behaviors [12]. The model uses exploration and exploitation techniques to optimize the hyperparameters of the F-RCNN and HKMBSVM models. The initial population denotes the candidate solutions (hyperparameter sets) and is randomly distributed with the search space range. This process is given as

$$rb_{p,q} = LB + (UB - LB).rand(0,1) \tag{24}$$

Here, $LB\ and\ UB$ denotes the lower and upper bounds values, and $rand$ denotes the random number between $0\ and\ 1$. The food search phase in the RBMO algorithm emulates the adaptive foraging behavior of red-billed blue magpies. The algorithm splits search techniques into small groups and clusters for exploration and efficiency. When a small group (2-5 magpies) explores for food, the new position of each search agent (SA) is computed using,

$$RB_p(t+1) = RB_p(t) + \left(\frac{1}{N_S}\sum_{m=1}^{N_S} \quad RB_m(t) - RM_{rs}(t)\right) \times rand2 \tag{25}$$

Here, $RB_p(t+1)$ indicates the new location of the p^{th} SA in the next iteration, $RB_p(t)$ denotes the current position of the p^{th} SA, N_S denotes the number of magpies in the small group ($N_S \in [2,5]$), $RB_m(t)$ denotes the position of the m^{th}individuals that are selected randomly from the group, $RM_{rs}(t)$ denotes the position of a randomly chosen search agent from the entire population, and $rand2$ denotes a random scalar value generated between $0\ and\ 1$.

When the cluster (10 or more magpies) explores for food, the position update is given as

$$RB_p(t+1) = RB_p(t) + \left(\frac{1}{N_G}\sum_{m=1}^{N_G} \quad RB_m(t) - RM_{rs}(t)\right) \times rand3 \tag{26}$$

Here, N_G denotes the number of magpies in the cluster $(N_G \geq 10)$ and $rand3$ denotes a random scalar value generated between $0\ and\ 1$.

The attacking prey phase in the RBMO algorithm refines the position to get closer to the optimal solution using two techniques: small group attacking prey and larger cluster attacking prey. The small group attacking prey (2 to 5 magpies) position update is formulated as

$$RB_p(t+1) = RB_{os}(t) + CF \times \left(\frac{1}{N_S}\sum_{m=1}^{N_S} \quad RB_m(t) - RB_p(t)\right) \times r_{a1} \tag{27}$$

Here, $RB_{os}(t)$ denotes the position of the food (optimum solution till now), N_S denotes the number of magpies in the small group $(2 \leq N_S \leq 5)$, CF denotes the control factor to regulate the step size, and r_{a1} denotes the random number from a standard normal distribution. For clusters (more than 10), the position update is formulated as

$$RB_p(t+1) = RB_{os}(t) + CF \times \left(\frac{1}{N_G}\sum_{m=1}^{N_G} \quad RB_m(t) - RB_p(t)\right) \times r_{a2} \tag{28}$$

Here, N_G denotes the number of magpies in the cluster $(N_G \geq 10)$, r_{a2} denotes a random number from a standard normal distribution. CF factor value is defined as

$$CF = \left(1 - \frac{t}{T_{max}}\right)^{\left(2\times\frac{t}{T_{max}}\right)} \tag{29}$$

Here, t denotes the present iteration and T_{max} indicates the maximum number of iterations.

The food storage phase preserves the excess food for future use. This process retains the information about the optimum solution discovered in the optimization context. This method ensures the algorithm refers to the globally optimum solution while avoiding degrading fitness during exploration and exploitation. The search agent position is updated based on a comparison of the fitness values before and after the current update. This process is formulated as

$$RB_p(t+1) = \{RB_p(t),\ \ if\ fit_p^{old} > fit_p^{new}\ RB_p(t+1),\quad else \tag{30}$$

Here, fit_p^{old} denotes the fitness value of the p^{th} search agent before updating its position, and fit_p^{new} denotes the fitness value of the p^{th} search agent after updating its position.

4. Result and discussion

The OFRCN-HKMBSVM model for Pulmonary Disease detection used an IQ-OTH/NCCD dataset from Kaggle. The evaluation used Python on a PyCharm tool on a system with an Intel Core i5 processor, Windows 10 OS with 512GB SSD, and 8GB RAM. Accuracy, Precision, Recall, F1 score, MSE, MAE, RMSE, dice similarity coefficient (DSC), and Jaccard index (JI) are used for the analysis. Table I presents the experimental setup for the model.

Table 1. Experimental Setup

Parameters	**Values**
Number of layers	15
Learning rate	0.001
Drop our	0.5

Batch size	256
Weight decay	0.0001
ROI pooling size	7X7
RPN anchor ratios	[0.5,1,2]
IoU threshold for NMS	0.5
Soft margin	0.1
Kernel	hybrid
Regularization parameter	0.01
Margin (C)	10
Polynomial degree	4
Bessel kernel order	1
Polynomial coefficient	3
RBF sigma	2.0
Weight Polynomial	0.7

Table 2. Class-wise results for the OFRCN-HKMBSVM model

Class	**Accuracy (%)**	**Precision (%)**	**Recall (%)**	**F1 score (%)**
Normal	99.61	99.21	99.34	99.27
Bacterial Pneumonia	99.50	99.19	99.80	99.49
COVID19	99.59	99.82	99.57	99.69
Tuberculosis	99.55	99.91	99.49	99.70
Viral Pneumonia	98.45	98.93	98.89	98.90
Lung cancer	99.7	99.5	99.42	99.45

Table II presents the detection performance of the OFRCN-HKMBSVM model for various classes. The accuracy ranges from 98.45% to 99.7% for all the classes. The model demonstrated better outcomes for the metrics, which reduced misclassification. The OFRCN-HKMBSVM model outcomes are computed and compared using the SVM, F-RCNN, and CNN models.

Table 3. Comparison of OFRCN-HKMBSVM model with Existing models

Model	**Accuracy (%)**	**Precision (%)**	**Recall (%)**	**F1 score (%)**	**MSE**	**MAE**	**RMSE**	**DSC**	**JI**
SVM	90.25	89.63	91.29	90.45	0.5674	0.2458	0.8475	0.9314	0.7851
F-RCNN	92.01	90.94	91.34	91.13	0.6311	0.4713	0.9612	0.8956	0.8536
CNN	93.53	92.55	91.23	91.88	0.5927	0.3645	0.7461	0.9345	0.8321
OFRCN-HKMBSVM	**99.4**	**99.44**	**99.42**	**99.41**	**0.4104**	**0.1491**	**0.6407**	**0.9407**	**0.8899**

Table 4. Comparison of OFRCN-HKMBSVM model with Related works

Model	Dataset	Class	Accuracy (%)	Precision (%)	Recall (%)	F1 score (%)
CNN-XAI [3]	Public	COVID-19	90.23	89.51	96.56	92.97
		Normal	92.78	90.96	92.87	91.65
		Pneumonia	96.45	97.26	96.19	96.53
		TB	97.31	96.45	91.19	93.52
DNN [4]	chest X-ray	COVID-19	99.53	99.79	99.75	99.76
		Pneumonia	99.41	99.14	99.40	99.27
		TB	99.44	99.90	99.61	99.76
MCESEL [5]	Public	Pneumonia	98	98	98	98
		TB	99	99	99	99
		COVID-19	98	98	98	98
F-RNN-LSTM [6]	C13RD	COVID-19, Pneumonia	95.04	93.65	96.78	95.19
	CXIP	Viral, bacterial Pneumonia	94.31	88.89	95.41	92.03
DCSNN [7]	NIH Chest X-ray	Normal	96.25	93.61	97.74	91.09
		COVID-19	99.06	98.27	98.81	97.45
		Pneumonia	97.21	95.69	96.29	96.21
PulmoNet [8]	Public	bacterial Pneumonia	95	90.52	95.01	88.65
		COVID-19	93	95.15	98.54	97.34
		Viral Pneumonia	91	98.86	99.41	98.46
		Healthy	97	99.12	99.01	99.24
DWTMBConvNet [9]	Public	Normal, Viral Pneumonia, bacterial Pneumonia, COVID-19, and TB	95.5	98.9	95.5	95
BSD[10]	COVID-19	COVID-19	90.64	90.63	90.64	90.63
		Lung Capacity	93.82	93.81	93.82	93.82
		Normal	92.43	92.42	92.43	92.42
		Viral Pneumonia	95.62	95.62	95.62	95.61
OFRCN-HKMBSVM	**IQ-OTH/NCCD**	**Normal**	**99.61**	**99.21**	**99.34**	**99.27**
		Bacterial Pneumonia	**99.50**	**99.19**	**99.80**	**99.49**
		COVID-19	**99.59**	**99.82**	**99.77**	**99.79**
		TB	**99.61**	**99.91**	**99.49**	**99.70**
		Viral Pneumonia	**98.45**	**98.93**	**98.89**	**98.90**
		Lung cancer	**99.7**	**99.5**	**99.42**	**99.45**

Table III compares the OFRCN-HKMBSVM model outcomes with the standard models. The OFRCN-HKMBSVM model attained the increased accuracy of 99.4% compared to standard models. The model also exhibited a lower MSE of 0.4104 and RMSE of 0.6407, which improved prediction reliability. Table IV compares the OFRCN-HKMBSVM model with the existing models for different classes. The model achieved accuracy of 99.61%, 99.50%, 99.59%, 99.61%, 98.45% and 99.70% for tuberculosis (TB), Bacterial Pneumonia, lung cancer, Normal, COVID-19, and Viral Pneumonia, respectively. The model distinguished between multiple pulmonary diseases with minimal misclassification.

Fig 3 compares the OFRCN-HKMBSVM model with SVM, F-RCNN, and CNN models. The OFRCN-HKMBSVM consistently achieves the highest accuracy ranging of 99.4%, which is increased by 5.87% - 9.15 % than SVM, F-RCNN and CNN. The model demonstrates the robustness of the OFRCN-HKMBSVM model in distinguishing complex pulmonary diseases.

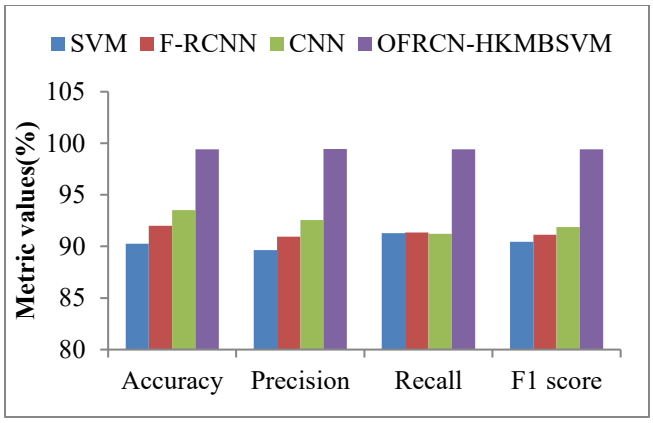

Fig 4. Comparison graph for evaluation metrics

Fig 4 illustrates the performance comparison MSE and MAE metrics of the OFRCN-HKMBSVM model with other models. The OFRCN-HKMBSVM has the lowest MSE of 0.4104 and RMSE of 0.6407, which indicates better prediction reliability.

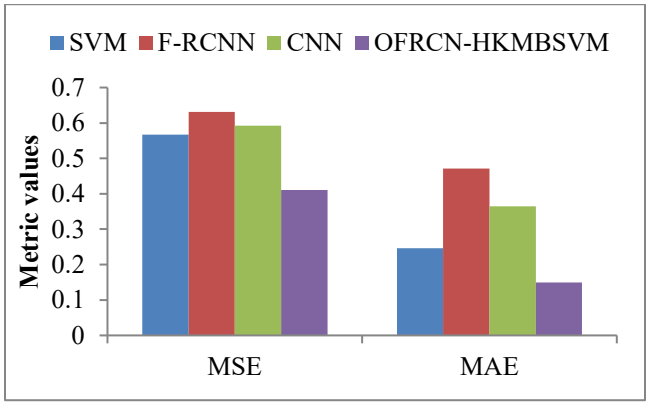

Fig 5. Comparison graph for MSE and MAE metrics

Fig 5 illustrates the performance comparison RMSE, DSC, and JI metrics of the OFRCN-HKMBSVM model with other models. The model attained Dice Similarity Coefficient (DSC) of 0.9407 and Jaccard Index (JI) of 0.8899 are the highest that has strong segmentation and classification capabilities. The model reduces classification errors compared to previous models.

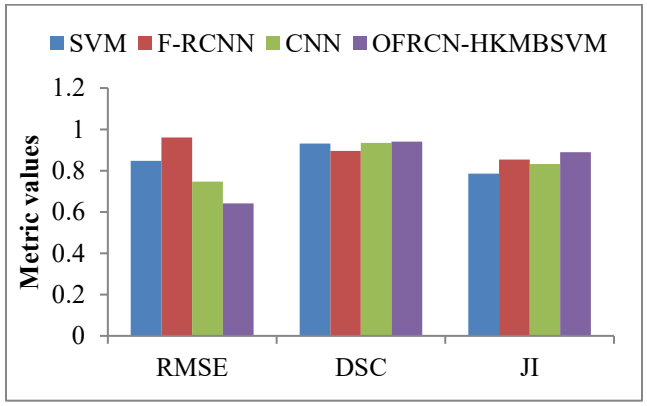

Fig 6. Comparison graph for RMSE, DSC and JI metrics

5. Conclusion

This paper developed an OFRCN-HKMBSVM model with advanced DL and ML methods for the accurate detection of lung cancer, tuberculosis, COVID-19, viral and bacterial pneumonia. The model combined F-RCNN for collecting the features and HKMBSVM for classification. The RBMO fine-tunes hyperparameters, reducing computational complexity, inference time, and resource requirements while enhancing detection precision. The integration of advanced feature extraction, detection, and optimization techniques makes OFRCN-HKMBSVM a robust and scalable diagnostic module for real-world medical applications.

REFERENCES

1. M. T. Barbosa, M. Morais-Almeida, C. S. Sousa, and J. Bousquet, "The "big five" lung diseases in COVID-19 pandemic–a Google Trends analysis", Pulmonology, vol. 27, no. 1, pp. 71-72, January 2021.
2. S. Kumar, H. Kumar, G. Kumar, S. P. Singh, A. Bijalwan, and M. Diwakar, "A methodical exploration of imaging modalities from dataset to detection through machine learning paradigms in prominent lung disease diagnosis: a review", BMC Medical Imaging, vol. 24, no. 1, p. 30, February 2024.
3. M. Bhandari, T. B. Shahi, B. Siku, and A. Neupane, "Explanatory classification of CXR images into COVID-19, Pneumonia and Tuberculosis using deep learning and XAI", Computers in Biology and Medicine, vol. 150, pp. 106156, November 2022.
4. M. K. Mahbub, M. Biswas, L. Gaur, F. Alenezi, and K. C. Santosh, "Deep features to detect pulmonary abnormalities in chest X-rays due to infectious diseaseX: Covid-19, pneumonia, and tuberculosis", Information Sciences, vol. 592, pp. 389-401, May 2022.
5. S. Goyal, and R. Singh, "Detection and classification of lung diseases for pneumonia and Covid-19 using machine and deep learning techniques. Journal of Ambient Intelligence and Humanized Computing, Vol. 14, No. 4, pp. 3239-3259, April 2023.
6. R. K. P. M. T. K. R. Rajagopal, R. Karthick, P. Meenalochini, and T. Kalaichelvi, "Deep Convolutional Spiking Neural Network optimized with Arithmetic optimization algorithm for lung disease detection using chest X-ray images", Biomedical Signal Processing and Control, vol. 79, pp. 104197, January 2023.
7. A. Mezina, and R. Burget, "Detection of post-COVID-19-related pulmonary diseases in X-ray images using Vision Transformer-based neural network", Biomedical Signal Processing and Control, vol. 87, pp. 105380, January 2024.
8. G. E. Rao, B. Rajitha, P. N. Srinivasu, M. F. Ijaz, and M. Woźniak, "Hybrid framework for respiratory lung diseases detection based on classical CNN and quantum classifiers from chest X-rays", Biomedical Signal Processing and Control, vol. 88, pp. 105567, February 2024.
9. A. M. Harale, V. K. Bairagi, E. Boonchieng, M. R. Bachute, "Nodules Detection in Lungs CT Images Using Improved YOLOV5 and Classification of Types of Nodules by CNN-SVM", IEEE Access, September 2024.
10. S. Yi, S. Qin, F. She, D. Shao, "BSD: A multi-task framework for pulmonary disease classification using deep learning", Expert Systems with Applications, Vol. 259, p. 125355, January 2025.
11. Z. X. Yang, Y. H. Shao, and X. S. Zhang, "Multiple birth support vector machine for multi-class classification", Neural Computing and Applications, vol. 22, pp. 153-161, May 2013.
12. S. Fu, K. Li, H. Huang, C. Ma, Q. Fan, and Y. Zhu, "Red-billed blue magpie optimizer: a novel metaheuristic algorithm for 2D/3D UAV path planning and engineering design problems", Artificial Intelligence Review, vol. 57, no. 6, p. 134, May 2024.